Identification of Dangerous LNG Sloshing Using a Rapid Sloshing Model Validated with Computational Fluid Dynamics

Bernhard Godderidge[a], *Stephen Turnock*[a], *Chris Earl*[b], *Mingyi Tan*[a]

[a]School of Engineering Sciences, Ship Science
University of Southampton.
Southampton, UK

[b]BMT SeaTech Ltd.
Southampton, UK

.

ABSTRACT

A non-linear pendulum model is developed to represent the motion of a sloshing fluid in real time. The forces imposed by the sloshing fluid are identified using multiphase RANS CFD simulations and subsequently included in the pendulum sloshing model. The pendulum sloshing model was used to simulate sloshing induced by linear and angular motions at and near resonance. Good agreement between the CFD data and the pendulum sloshing model was observed. A blind simulation with multiple surge excitation components is carried out and the pendulum sloshing model agrees with the RANS CFD result. Typically, the computational time of the pendulum is approximately 1/700th of real time.

KEY WORDS: Sloshing; multiphase; CFD; Simplified sloshing models; nonlinear pendulum

INTRODUCTION

Sloshing occurs when a tank is partially filled with a fluid and subjected to an external excitation force (Olsen, 1976). Ships with large ballast tanks and liquid bulk cargo carriers, such as very large crude carriers (VLCCs), are at risk of exposure to sloshing loads during their operational life (Rizzuto and Tedeschi, 1997). The inclusion of structural members within the tanks dampens the sloshing liquid sufficiently in all but the most severe cases. However, this approach is not used for Liquefied Natural Gas (LNG) carriers and the accurate calculation of the sloshing loads is an essential element of the LNG tank design process (Bass et al., 1980; Knaggs, 2006). Recent increases in vessel size have renewed interest in methodologies for the simulation of the sloshing loads experienced by the containment system (Han et al., 2005; Card and Lee, 2005).

While the sloshing response depends on the amplitude and frequency of the excitation force, history effects can be of significance as well. Waterhouse (1994) observed the hard and soft spring-type behavior of a sloshing flow. The offset of the response peak from the resonant excitation was found to depend on the tank filling level.

The work of Abramson (1966) summarizes the methods available in modern sloshing analysis, and Ibrahim (2005) gives an up-to-date survey of analytical and computational sloshing modeling techniques. A more general modeling technique is the solution of the Navier-Stokes equations using Computational Fluid Dynamics (CFD). Some recent examples of CFD sloshing simulation include Hadzic et al. (2002), Aliabadi et al. (2003), Standing et al. (2003) and El Moctar (2006).

Sloshing flows are treated as a transient problem in CFD. While the number of sloshing oscillations can vary, a large number of time steps, usually $O(10^2)$ to $O(10^3)$ per oscillation are required. Design optimization or the use of a numerical wave tank to gather statistical sloshing pressure data (Graczyk et al., 2006) require long simulation times or multiple runs.

The associated computational requirements make the use of a three dimensional CFD model impractical for such studies. There is still a requirement for the development of simplified mathematical sloshing models. These models operate in faster than real time (fast time) and can be used to provide sufficiently long time series for statistical analysis. Faltinsen et al. (2000, 2001, 2002) use a potential flow model and develop a multimodal system to describe sloshing in a rectangular container. Reported computational times for two dimensional sloshing are less than 1% of real time (Faltinsen et al., 2000).

Phenomenological modeling is another approach for the development of a simplified sloshing model. Rather than solving a detailed mathematical description of the flow, the forces acting on the system are approximated and included in a mathematical model. Schlee et al. (2005) proposed a MATLAB-based model to determine the characteristics of a pendulum sloshing model based on experimental data.

The approach adopted in this study is to analyze the detailed fluid loading occurring during sloshing based on a validated CFD sloshing model. This allows the construction of mathematical models for the individual force components and other associated terms. These are then incorporated in a pendulum sloshing model. This model is tested using regular linear excitations at and near resonance. Angular motions are then investigated. Finally, the blind simulation of sloshing with multiple simultaneous excitations presents a test of realistic motions.

SLOSHING PROBLEM

Membrane tanks are considered to be at greater risk from sloshing damage than spherical tanks. Although a tank will experience motions in all six degrees of freedom, the most severe are roll, pitch, sway and surge (Lloyds Register, 2005). The initial CFD analysis is normally undertaken by considering two dimensional sloshing motions of the longitudinal and transverse cross sections of the tank (Lloyds Register, 2005). In this study only the longitudinal (rectangular) cross section is considered.

Tank Geometry

The longitudinal cross-section of a membrane tank is shown in Fig. 1. The dimensions of the tank are scaled to coincide with the experiment by Hinatsu (2001). A 60% filling level is used in the simulation. The resonant frequencies of a rectangular tank are calculated using potential flow (Abramson, 1966)

$$\omega_m^2 = gk \tanh(kh),\qquad(1)$$

where g is gravity, h the filling depth and, for a two dimensional tank

$$k^2 = \pi^2\left(\frac{m^2}{a^2}\right),\qquad(2)$$

where a is the length of the tank and $m = 1,2,3,...,\infty$. Usually, the first $(m=1)$ resonant frequency is the most crucial. Both linear and angular excitations are investigated.
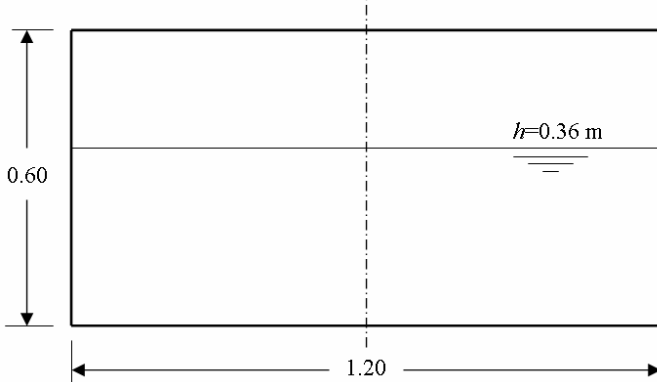

Fig. 1: Longitudinal tank cross section. *All dimensions in m*

NUMERICAL MODEL

Governing Equations

Multiphase CFD is established as a suitable methodology for the study of sloshing flows. An inhomogeneous multiphase model, which includes separate transport equations for mass, momentum and energy for every fluid provides a more faithful representation of the dynamic interaction between the fluids (Ishii and Hibiki, 2006). A full set of conservation equations is solved for each phase:

$$\frac{\partial}{\partial t}(r\rho) + \frac{\partial}{\partial x_i}(r\rho u_i) = m + \Gamma\qquad(3)$$

and

$$\frac{\partial}{\partial t}(r\rho u_i) + \frac{\partial}{\partial x_j}(r\rho u_i u_j) = -r\frac{\partial p}{\partial x_i} + \frac{\partial \tau_{ij}}{\partial x_j} + M^\Gamma + M^r + b_i,\qquad(4)$$

and the stress tensor τ_{ij} is written as

$$\tau_{ij} = \mu\left(\frac{\partial u_i}{\partial x_j} + \frac{\partial u_j}{\partial x_i}\right),\qquad(5)$$

where b_i is external body force (e.g. gravity), Γ mass transfer, μ dynamic viscosity, M^Γ momentum transfer due to mass transfer, M^r forces on the interface caused by the presence of the other phase, ρ density, p pressure, r volume fraction, u_i and x_i the Cartesian velocity and co-ordinate tensors. The mass and momentum transfer terms link the phase velocity fields. In the present problem there is no interphase mass transfer and the only remaining term is M^r. This is computed using the relative velocity between the liquid and gas phases.

In the more widely used homogeneous multiphase model, this term is assumed to be large and hence there is no relative velocity between the phases (Brennen, 2005). Consequently, only one set of momentum conservation equations has to be solved. This reduces computational effort by typically 60% (Godderidge et al., 2007b). However, Godderidge et al. (2007b) found that when simulating a nonlinear sloshing flow using CFD, the more complex inhomogeneous multiphase model should be used.

Discretization

The governing equations are discretized using a finite volume method. Zwart (2004) describes the discretization procedure, gives the governing equations in their discretized form and describes the solution strategy. The advection scheme is based on the scheme by Barth and Jesperson (1989) and the free surface is compressed by introducing an anti-diffusive flux in cells near the fluid interface (Zwart, 2004; ANSYS, 2007).

The numerical investigations were carried out using the commercial CFD code CFX-11.0[1]. The grid used for the longitudinal cross-section (rectangular tank) is shown in Fig. 2. A total of 8,745 elements (8,109 hexahedral and 636 wedge) are used and the refined region at the top corners contains 5,266 hexahedral elements. The advantage of the hybrid grid used in this study is that only the regions of interest were refined while maintaining a hexahedral-dominant grid. This resulted in
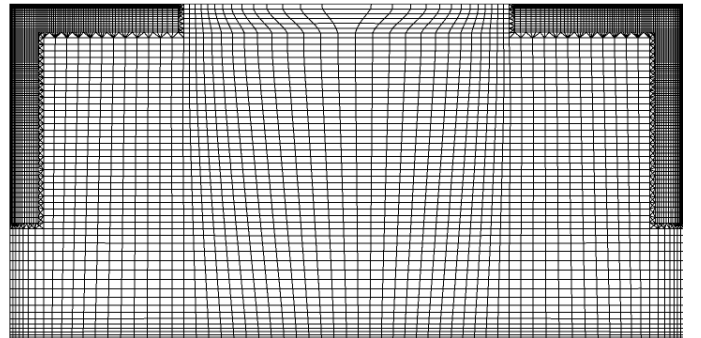

Fig. 2: Computational grid used for the rectangular cross-section

a more efficient use of computational resources. Table 1 summarizes

---

the computational parameters used. The selection is based on the sensitivity studies by Godderidge et al. (2006, 2007b).

Table 1: CFD model description and parameters

Parameter	Setting
Water	Incompressible fluid
Air	Ideal gas
Sloshing motion	Body force, rotating frame of reference
Turbulence model	Standard k-ε with scalable wall function
Spatial discretization	Gradient-dependent first or second order
Temporal discretization	Second order backward Euler
Timestep control	Root-mean-square (RMS) Courant number=0.1
Convergence control	RMS residual $< 10^{-5}$

The high resolution scheme for spatial discretization varies between a first and second order upwind scheme depending on the gradient (ANSYS, 2007). It was found to be the most stable scheme. The sloshing motion of the container was applied using a body force approach. This approach adds additional time-dependent terms in the external body force vector b_i for linear motions. When the tank is subjected to rotational motions, additional forces are introduced. These are accounted for with the introduction of corresponding terms in the conservation of momentum Equation (4) (ANSYS, 2007).

RAPID SLOSHING MODEL

Pendulum Equation

Sloshing is the motion of a fluid due to excitations imparted through the motion of its container. The behavior of the fluid can be represented using equations of motion (e.g. Equations 3 and 4). A popular phenomenological approximation is the pendulum model. Fig. 3 shows the forces acting on a linearly damped pendulum with an excitation body force $A(t)$. The resulting equation describing the pendulum motion is determined using Newton's second law

Fig. 3: Damped forced pendulum

$$\ddot{\theta} = -\beta\dot{\theta} - \frac{g}{l}\sin(\theta) + \frac{1}{l}A(t)\cos(\theta),\qquad(6)$$

where $A(t) = A\sin(\omega t)$ is the excitation with frequency ω, β a damping coefficient, g gravity, l and m pendulum length and mass respectively, θ angular displacement and ω excitation frequency. Time derivatives are indicated by superscript dots.

Although the pendulum model has been used previously to simulate sloshing (Aliabadi et al, 2003), the significance of individual terms warrants closer scrutiny. The first term $-\beta\dot{\theta}$ is the damping force acting on the pendulum. The gravity term $-\frac{g}{l}\sin(\theta)$ is a restoring force,
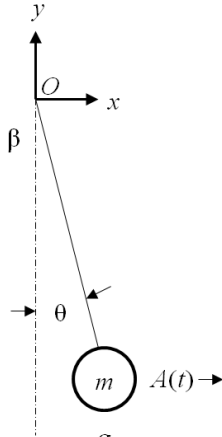
countering the lateral pendulum body force.

Fluid Motion in a Sloshing Tank

As a pendulum models the sloshing fluid as a single moving mass, the behavior of fluid integral quantities needs to be considered. The path of the fluid centre of gravity for different excitation periods, given relative to the first natural period T_1 with a horizontal excitation amplitude of $0.0125L$ calculated using the CFD model outlined previously, are compared in Fig. 4. For the range of frequencies shown, the centre of gravity appears to follow the same path.
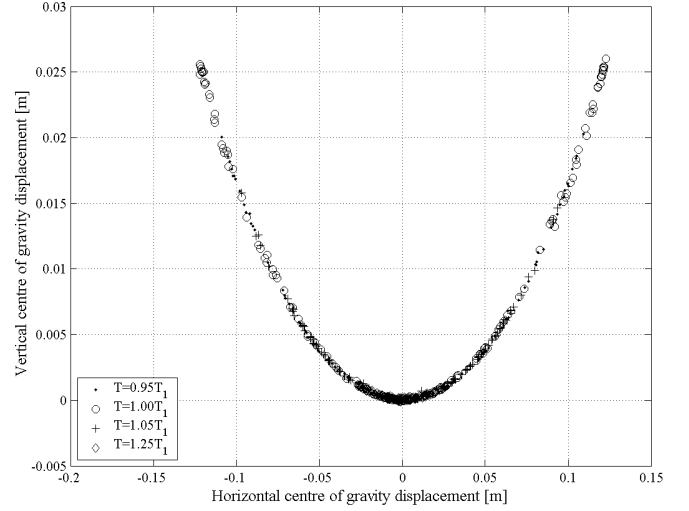

Fig. 4: Displacement of the fluid centre of gravity caused by linear horizontal tank excitation
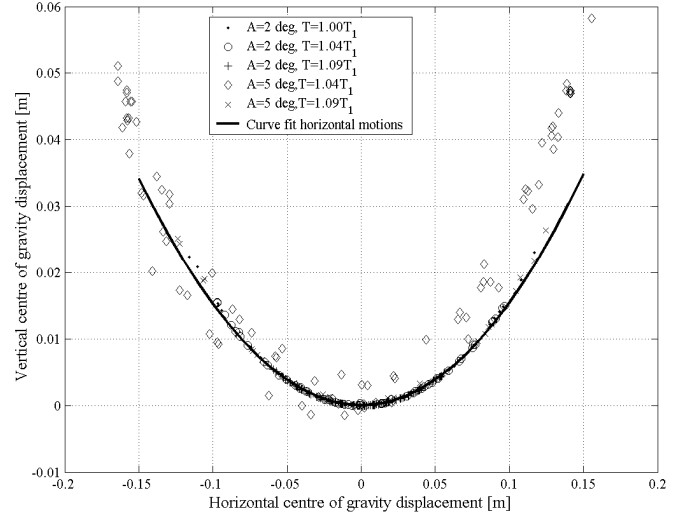

Fig. 5: Displacement of the fluid centre of gravity caused by angular tank excitation

Similar observations can be made in Fig. 5 for angular excitations. The centre of gravity follows the same path observed in Fig. 4 for two and five degree excitation amplitudes. The near-resonance flow with excitation amplitude of five degrees includes fluid fragmentation and overturning. This results in greater scatter of the fluid centre of gravity displacement.

Sloshing Tank Forces

Viscous Forces at the Wall. The formation of boundary layers at the tank walls affects the sloshing motion. Its impact is generally considered small (Bass, 1980) and viscous effects are frequently neglected. However, the inclusion of viscosity is observed to influence the long-term behavior of sloshing simulations (Cariou and Casella, 1999).
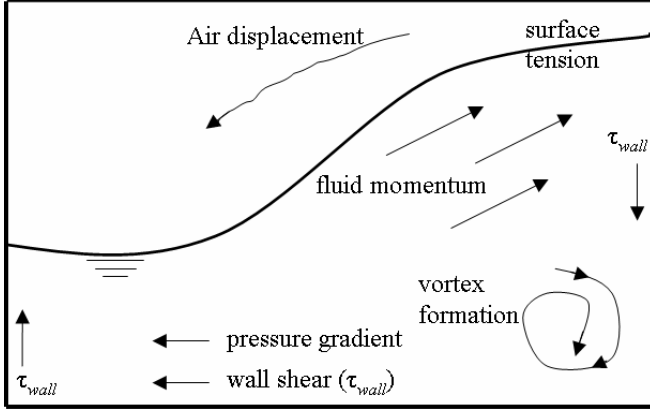

Fig. 6: Forces acting on the fluid due to sloshing

The laminar viscous boundary layer formed over an oscillating plate and the flow over an accelerating plate are two solutions that have a degree of applicability to the to the wall boundary layer observed during sloshing. They can be used to model the effect of viscous dissipation in a sloshing model. The laminar viscous flow over an oscillating plate, which has been compared to a sloshing boundary layer (Godderidge et al, 2007a), can be written as

$$u(z,t) = U_0 \exp\left(-z\sqrt{\frac{\omega}{2\nu}}\right)\cos\left(\omega t - z\sqrt{\frac{\omega}{2\nu}}\right), \qquad (7)$$

where ν is the kinematic viscosity, U_0 plate velocity, $\omega = 2\pi/T$ frequency and z depth. The viscous shear stress at the wall is given as

$$\tau_{wall} = \mu \frac{\partial u}{\partial z}\bigg|_{z=0} . \qquad (8)$$

Replacing u with Equation (7) gives

$$\tau_{wall} = \mu\left[\frac{1}{2}U_0\sqrt{\frac{2\omega}{\nu}}(\sin\omega t - \cos\omega t)\right]. \qquad (9)$$

The wall shear force is linearly proportional to velocity, which is analogous to the damping force in Equation (6). However, the wall shear stress also depends on the square root of the frequency of excitation.

The velocity profile of an accelerating plate is a better approximation of the boundary layer formed during sloshing (Godderidge et al, 2007a). The first approximation is developed by Schlichting (1960) as

$$u(z,t) = U(x)erfc\left(\frac{y}{2\sqrt{\nu t}}\right), \qquad (10)$$

where $erfc\left(\dfrac{y}{2\sqrt{\nu t}}\right)$ is the complementary error function. This velocity profile again leads to a linear relation between shear stress and fluid velocity. However, the second approximation of the two-dimensional case (Schlichting, 1960) includes non-linear fluid velocity terms. A linear relation between fluid velocity and viscous dissipation, appears sufficient, but the inclusion of higher order damping may be necessary in a more detailed model.

Viscous Dissipation. The effects of fluid viscosity are not confined to the boundary layer region. Dissipation occurs in the body of the fluid and, if it is contaminated with another fluid (e.g. oil on water), at the free surface. However, Keulegan (1958) observes that the viscous dissipation in the fluid is negligible compared the boundary layer.

The velocity dependence of the viscous forces on the wall can therefore be used to determine a suitable damping model. Keulegan (1958) develops a linear damping model for viscous dissipation of a standing wave in a rectangular tank, which is synonymous with sloshing at higher filling levels (Lloyds Register, 2005). The viscous dissipation in the linear model depends on the square root of the excitation frequency and kinematic viscosity. For a two dimensional tank, the linear damping model from Keulegan (1958) gives the damping coefficient β as 0.0036 s^{-1} at resonance, compared to 0.0050 s^{-1} measured from the logarithmic decrement of a sloshing simulation.

Violent sloshing flows can experience fluid impact opposing the flow velocity. A third order damping model is chosen to account for fluid impacts and the corresponding damping coefficient is computed as $\beta_3 = 0.14$. It was obtained by computing the decay during one impact and reproducing it using an appropriate damping function.

Pressure Imbalance Force. As the fluid moves from its equilibrium position in its container, a horizontal pressure gradient develops. This pressure gradient opposes the motion of the fluid and acts as a restoring function. Fig. 7 shows the longitudinal pressure gradient observed in the CFD computations for linear excitations with displacement amplitude of $0.0125L$ and angular excitations at two and five degrees amplitude. The angles are measured from the centre of the tank. Although there is some spread at the maximum angle, the gradient at small angles is similar for the flows shown.
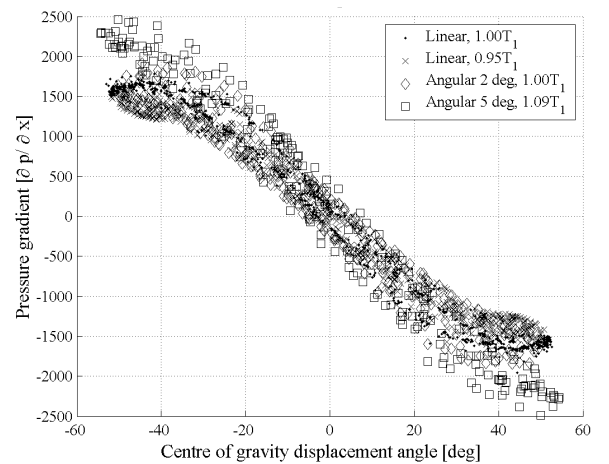

Fig. 7: Horizontal pressure gradient observed during linear and angular sloshing

Similarly, the pendulum is subjected to a force opposing its disturbance. In a nonlinear pendulum, this function is $mg \sin(\theta)$. The pressure gradient in Fig. 7 can be related to a restoring force by

$$F = \frac{m_{eff}}{\rho} \frac{\partial p}{\partial x},$$ (11)

where m_{eff} is the effective sloshing mass which is taken as $0.7 m_{fluid}$ (Abramson, 1966). Thus, the conventional pendulum force can be replaced by a function describing the pressure gradient-induced restoring force.
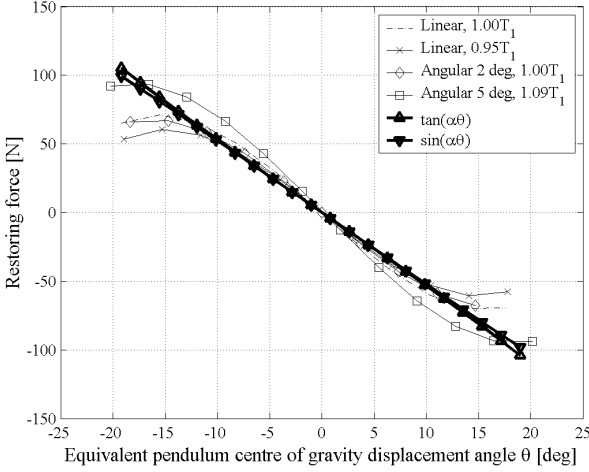

Fig. 8: Restoring function computed from pressure gradients

The restoring force is shown in Fig. 8. The angle is computed by moving the reference point from the tank centre to one pendulum length above the fluid centre of gravity. The observed restoring forces are obtained by fitting a third-order polynomial to the results from Eqn (11) using the data in Fig. 7. Both $\sin(\alpha\theta)$ and $\tan(\alpha\theta)$ are included as displacement functions. The tangent function is more representative of the sloshing flow without impact. Although the sine is better suited for large fluid displacements, both functions use $\alpha = 1.0225$.

Rotational Motion. Rotational excitations are modeled using a rotating frame of reference. The gravity vector moves according to the prescribed angular displacement $\theta = C \sin(\omega t)$, where C is the displacement amplitude. However, the use of a moving frame of reference gives rise to additional forces: a Coriolis force,

$$F_{CO} = -2m\vec{\dot{\theta}} \times \vec{u}_{rot}$$ (12)

where u_{rot} is the velocity in the rotating frame and a centrifugal force,

$$F_{CE} = -m\vec{\dot{\theta}} \times \left(\vec{\dot{\theta}} \times \vec{r}\right).$$ (13)

However, this does not consider the angular accelerations. The Euler force

$$F_E = -m\vec{\ddot{\theta}} \times \vec{r}$$ (14)

takes the unsteadiness of the angular motion into account (Batchelor, 1967). When the angular displacement amplitude is small, the Euler force is dominant. In the current investigations, the angular displacement amplitude will not exceed five degrees and the Coriolis

and centrifugal forces can be neglected.

The rotational forces depend on the spatial distribution of the sloshing liquid. Therefore an acceleration corresponding to each force is required for the pendulum sloshing model. In the CFD simulation the Euler force is

$$F_E = -\sum_i \left\| m_i \vec{\ddot{\theta}} \times \vec{r}_i \right\|$$ (15)

for i control volumes. Using a similar approach to the pressure gradient, the corresponding Euler acceleration is

$$A_E = \frac{F_E}{m_{eff}}.$$ (16)

The same approach can be taken if the Coriolis and centrifugal forces need to be included as well.

Pendulum Sloshing Model. Using the results obtained in this section, the pendulum equation (6), the governing equation can be re-written as

$$\ddot{\theta} = -\beta_3 \dot{\theta}^3 - \beta\dot{\theta} + \frac{1}{l}\left[- g \sin(\alpha\theta) + A(t)\right]$$ (17)

for linear excitations and

$$\ddot{\theta} = -\beta_3 \dot{\theta}^3 - \beta\dot{\theta} + \frac{1}{l}\left[\begin{array}{l} g \sin(\alpha\theta)\cos(C \sin \omega t)+ \\ + g \cos(\theta)\sin(C \sin \omega t) \end{array}\right] - A_E - A_C$$ (18)

This model is now compared to the RANS CFD model. The pendulum length l is calculated so that the resonant frequency of the undamped pendulum, given as

$$\omega_n = \sqrt{\frac{g}{l}},$$ (19)

coincides with the first resonant sloshing frequency.

TWO DIMENSIONAL SLOSHING

Linear Excitation

The initial test of the pendulum sloshing model is sloshing induced by horizontal tank motions at resonance, shown in Fig. 9 and greater than resonance, shown in Fig 10. The resonant sloshing includes fluid impacts at the top wall. The fluid momentum obtained from the RANS CFD model is compared to the pendulum sloshing model (Eqn.17) and the basic pendulum Equation (6).

The modified pendulum gives a good match to the magnitude of fluid momentum of the resonant sloshing flow in Fig. 9. However, the pendulum sloshing model starts to lead the sloshing flow. This may be attributable to fluid impacts at the top wall, which are observed throughout the CFD simulation. The second case with an excitation greater than resonance is well predicted by the pendulum sloshing model. The predicted momentum history remains in phase with the CFD data and the peaks, which vary throughout the simulation, are estimated with good accuracy.

However, the basic pendulum underestimates the fluid momentum at resonance and it fails to match the non-periodic fluid momentum history for the sloshing flow shown in Fig. 10. Neither the frequency of the signal nor the magnitudes of the peaks are estimated correctly.
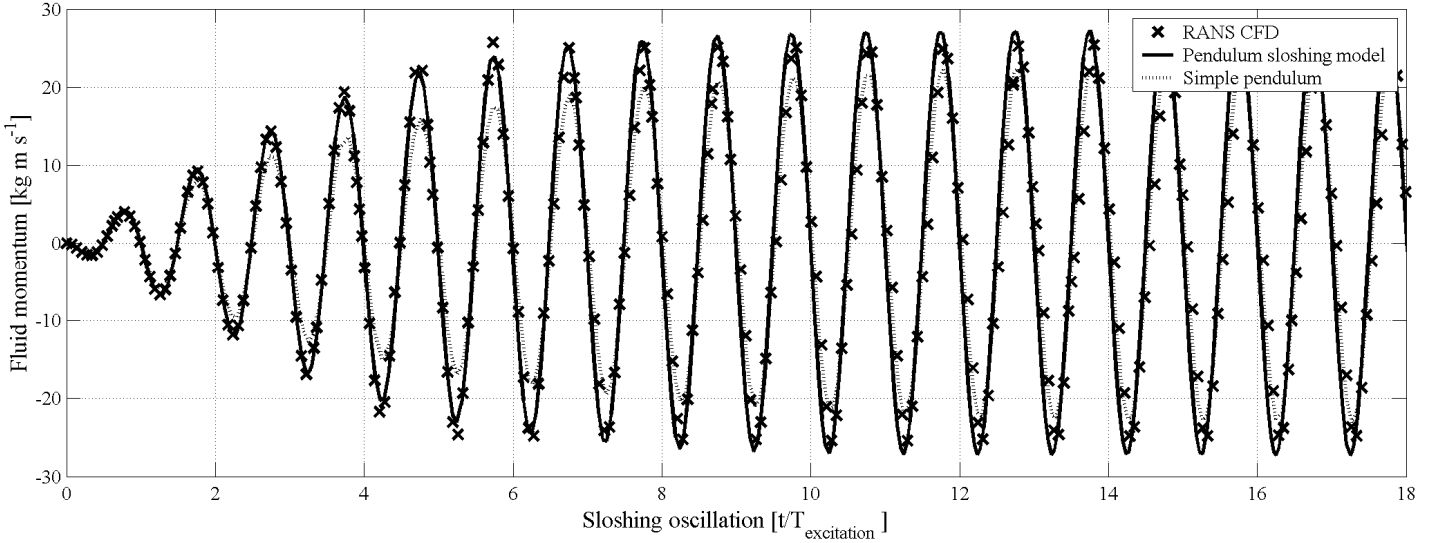
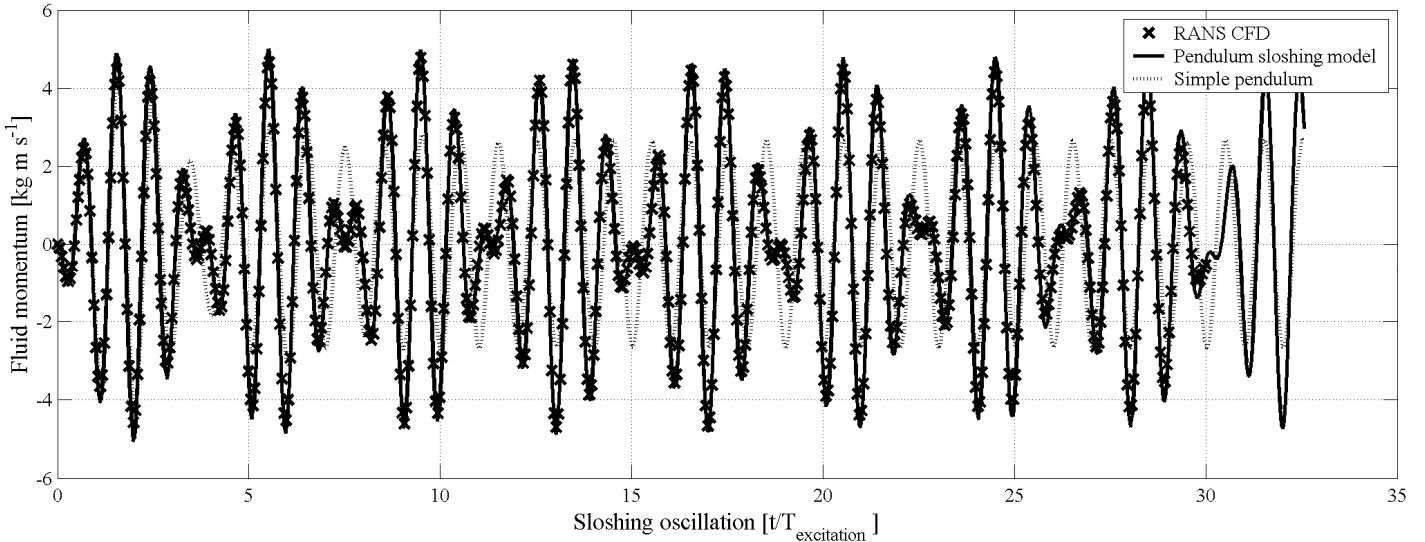Fig. 9: Fluid momentum history for sloshing induced by horizontal tank motions at resonance ($1.00T_1$)

Fig: 10: Fluid momentum history for sloshing induced by horizontal tank motions at $1.25T_1$

Angular Motions

Sloshing induced by angular tank motions constitutes the second test of the pendulum sloshing model. Fig. 11 shows the fluid momentum history of a flow excited by an angular excitation with a two degree amplitude and $1.09T_1$. The pendulum sloshing model described by Equation (18) predicts the momentum history well, with both plots remaining in phase.

There are some noticeable differences at the first oscillation and the trough at oscillation 10. The significance of the Euler force is illustrated in Fig. 11, where the absence of the Euler force results in an unrealistic momentum history. The influences of the Coriolis and centrifugal forces were nearly two orders of magnitude less than the Euler force and, when included, they have been found to be insignificant.

A more violent flow with tank ceiling impacts is depicted in Fig 12.

There is reasonable agreement between the pendulum sloshing model and the CFD model once the flow progresses past the initial transient phase. However, the first four peaks are not modeled with sufficient accuracy. This may be attributable to the absence of a separate model for fluid impacts, which are a key feature of this flow field.

Combined Linear Motions

The final case is a blind simulation of surge-induced sloshing with multiple excitations. The coefficients determined previously are used in the pendulum sloshing model for linear excitations given by Eqn (17). The excitation consists of four horizontal excitation components of the form

$$A(t) = \sum_{i=1}^{4} A_i \sin\left(\frac{2\pi}{B_i T_1} t \right), \tag{20}$$

where $A_1 = 8$, $A_2 = 4$, $A_3 = 2$, $A_4 = 1$, $B_1 = 1$, $B_2 = 1.05$, $B_3 = 1.5$,

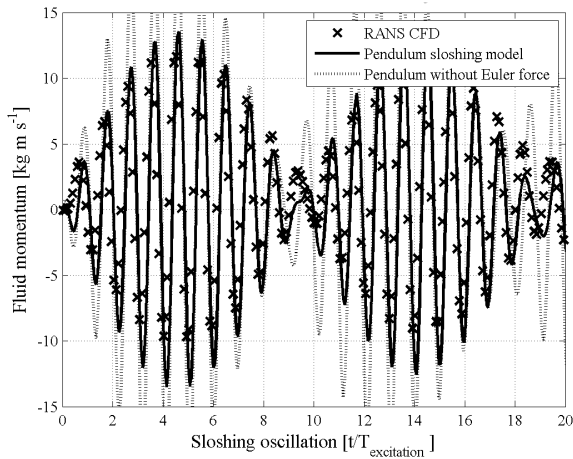Fig 11: Angular tank motions of 2 deg at $1.09T_1$
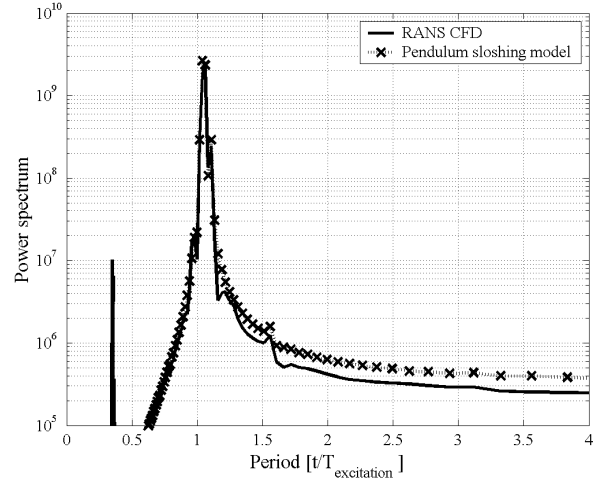

Fig 12: Angular tank motions of 5 deg at $1.04T_1$

Fig. 14: Power spectrum of momentum history and $B_4 = 3$.

Fig. 13 compares the fluid momentum history to the CFD result. There is generally good agreement and both histories remain in phase. The momentum in the initial transient period of about 10 s is underestimated by the pendulum sloshing model. However, after the initial transient, the pendulum sloshing model and the multiphase CFD result are in good agreement, with the differences less than 5%.

The spectrum of the momentum histories in Fig. 14 shows that the peak at $1.00T_1$ is predicted well with the pendulum sloshing model. Similarly, the peak at $1.05T_1$ is predicted reasonably well. The third excitation period at $1.50T_1$ is overestimated somewhat and the final component at $3.00T_1$ is not recognized in either the pendulum sloshing model or the CFD simulation. There is a high-frequency spike in the CFD data that is not reproduced by the pendulum sloshing model, however, its energy content is negligible.
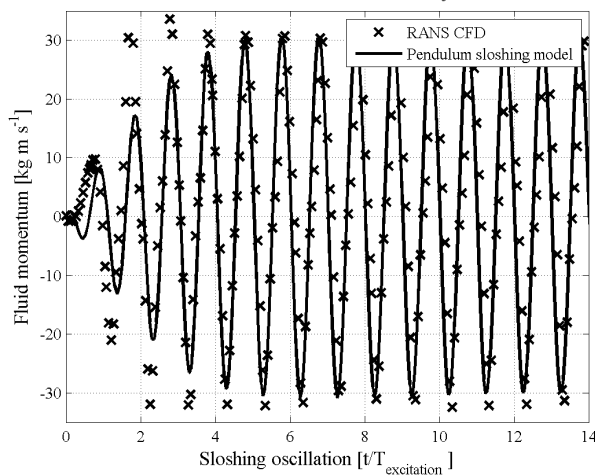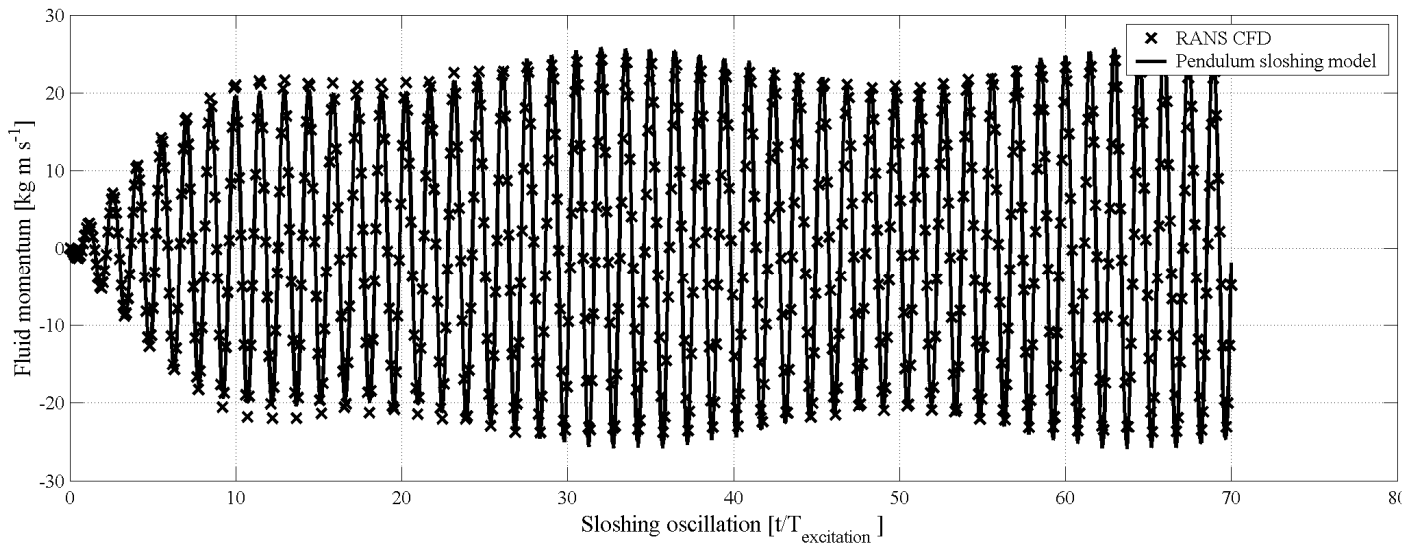

Fig. 13: Fluid momentum history for sloshing excited by multiple horizontal tank motions

CONCLUSIONS

RANS CFD can provide accurate sloshing pressure data but the associated time penalties are often prohibitive. Therefore, a simplified sloshing model, based on a pendulum equation, has been developed. It has been found that the physics governing a sloshing flow need to be modeled correctly to provide realistic results. The influence of damping was found to be small for sloshing with no fluid impact. The restoring force proved to be influential, especially when the flow history is not periodic.

When simulating a sloshing flow with multiple excitations, the pendulum sloshing model was able to reproduce the unique flow history as well as the power spectrum obtained from CFD. Fluid impacts on walls have been found to influence the restoring function and damping. The development of a model incorporating fluid impacts appears to be necessary for a more accurate representation of violent sloshing.

Initial tests of the pendulum sloshing model are promising and a blind simulation of sloshing with tank ceiling impacts was in good agreement with the CFD data. Further investigations of more complicated combinations of linear and angular excitations and variations in tank shape and filling level are currently being conducted. Finally, a realistic six-degree-of-freedom sloshing tank with pump tower will be analyzed with the pendulum sloshing model.

The principal strengths of this sloshing model are its simplicity, flexibility and speed. One hour simulation (approximately 2,400 oscillations) can be computed on a desktop PC in approximately five seconds of real time. Objects such as pump towers can be incorporated by assessing their influence on the damping and restoring force functions. This permits the rapid evaluation of the sloshing characteristics of a tank in a seaway taking history effects into account as well as the real time assessment of sloshing severity in LNG cargo tanks.

REFERENCES

Abramson, HN (1966). The dynamic behavior of liquids in moving containers with applications to space vehicle technology. *Report SP-106*, National Aeronautics and Space Administration.

Aliabadi, S, Johnson, A, and Abedi, J (2003). Comparison of finite element and pendulum models for simulation of sloshing. *Computers and Fluids*, Vol 32 pp 535–545.

ANSYS Inc (2007). ANSYS CFX-11 User's Guide.

Barth, TJ and Jesperson, DC (1989). The design and application of upwind schemes on unstructured meshes. AIAA Paper 89-0366.

Bass, RL, Bowles, EB and Cox, PA (1980). Liquid dynamic loads in LNG cargo tanks. *SNAME Transactions*, vol 88, pp 103–126.

Batchelor, GK (1967). An Introduction to Fluid Dynamics. Cambridge University Press, London.

Brennen, CE (2005). Fundamentals of Multiphase Flow, Cambridge University Press, New York.

Card, J and Lee, H (2005). Leading Technology for Next Generation of LNG Carriers. *Proc 15th International Offshore and Polar Engineering Conference.*

Cariou, A and Casella, G (1999). Liquid sloshing in ship tanks: a comparative study of numerical simulation. *Marine Structures*, vol 12, pp 183–198.

El Moctar, O (2006). Assessment for tankers. *Shipping World and Shipbuilder*, vol 204, pp 28-31.

Faltinsen, OF, Rognebakke, OF, Lukovsky, IA and Timokha, AN (2000). Multidimensional modal analysis of nonlinear sloshing in a rectangular tank with finite water depth. *Journal of Fluid Mechanics*, vol 407, pp 201–234.

Faltinsen, OF and Timokha, AN (2001). An adaptive multimodal approach to nonlinear sloshing in a rectangular tank. *Journal of Fluid Mechanics*, vol 432, pp 167–200.

Faltinsen, OF and Timokha, AN (2002). Asymptotic modal approximation of nonlinear resonant sloshing in a rectangular tank with small fluid depth. *Journal of Fluid Mechanics*, vol 470, pp 319–357.

Godderidge, B, Tan, M, Turnock, S and Earl, C (2006). Multiphase CFD modelling of a lateral sloshing tank. *Proc 9th Numerical Towing Tank Symposium Nantes.*

Godderidge, B, Tan, M, Earl, C and Turnock, S (2007a). Boundary layer resolution for modeling of a sloshing liquid. *Intl Soc Offshore and Polar Engrs Conf.*

Godderidge, B, Turnock, S, Tan, M and Earl, C (2007b) An Investigation of Multiphase CFD modelling of a lateral sloshing tank. *Computers and Fluids (in print).*

Graczyk, M, Moan, T and Rognebakke, O (2006) Probabilistic Analysis of Characteristic Pressure for LNG Tanks. *Journal of Offshore Mechanics and Arctic Engineering*, vol 128, pp 133-144.

Hadzic, I, Mallon, F, and Peric, M (2001). Numerical simulation of sloshing. *Proc of SRI-TUHH mini-Workshop on Numerical Simulation of Two-Phase Flows*. National Maritime Research Institute & Technische Universität Hamburg-Harburg.

Han, S, Heo, J-H and Lee, S-G (2005). Critical Design Issues of New Type and Large LNG Carriers. *Proc 15th International Offshore and Polar Engineering Conference.*

Hinatsu, M (2001). Experiments of two-phase flows for the joint research. Proc of SRI-TUHH *mini-Workshop on Numerical Simulation of Two-Phase Flows*. National Maritime Research Institute & Technische Universität Hamburg-Harburg.

Ibrahim, RA (2005). *Liquid Sloshing Dynamics*. Cambridge University Press.

Ishii, M, and Hibiki, T (2006), Thermo-Fluid Dynamics of Two-Phase Flow, Springer Verlag.

Keulegan, GH (1958). Energy dissipation in standing waves in rectangular basins. *Journal of Fluid Mechanics*, vol 6, pp 33-50.

Knaggs, T (2006). New strides in ship size and technology. Gas Ships: Trends and Technology, vol 2, pp 1-4.

Lloyds Register (2005). Comparative sloshing analysis of LNG ship containment systems. *ShipRight Additional Design Procedures.*

Olsen, O (1976). What is sloshing? *Seminar on Liquid Sloshing*. Det Norske Veritas.

Rizzuto, E and Tedeschi, R (1997). Surveys of actual sloshing loads onboard of ships at sea. *NAV 97: International Conference on Ship and Marine Research*, pp 7.29–7.37.

Schlichting,H (1960). Boundary Layer Theory, 4th ed. McGraw-Hill.

Schlee, K, Gangadharan, S, Ristow, J, Sudermann, J, Walker, C and Hubert, C (2005). Modeling and Parameter Estimation of Spacecraft Fuel Slosh Mode. Proceedings of the 2005 Winter Simulation Conference, pp 1265-1273.

Standing, RG, Amaratunga, S, Lopez-Calleja, F, Orme, S, and Eichaker, R (2003). Marine hydrodynamics modelling using CFD. *CFD 2003: Computational Fluid Dynamics Technology in Ship Hydrodynamics*, pp 1–12.

Waterhouse, DD (1994). Resonant sloshing near a critical depth. *Journal of Fluid Mechanics*, vol 281, pp 313-318.

Zwart, PJ (2004). Numerical modelling of free surface and cavitating flows, Industrial two-phase flow CFD: von Karman Institute Lecture Series 2004-2005, vol 25.